Received: 31 December 2021 | Revised: 30 July 2022 | Accepted: 13 August 2022

DOI: 10.1002/hbm.26069

RESEARCH ARTICLE

WILEY

The role of the parahippocampal cortex in landmark-based distance estimation based on the contextual hypothesis

Qunjun Liang | Jiajun Liao | Jinhui Li | Senning Zheng | Xiaoqian Jiang | Ruiwang Huang

School of Psychology, Center for Studies of Psychological Application, Guangdong Key Laboratory of Mental Health and Cognitive Science, Ministry of Education Key Laboratory of Brain Cognition and Educational Science, South China Normal University, Guangzhou, Guangdong, China

Correspondence
Ruiwang Huang, School of Psychology, South China Normal University, Guangzhou 510631, China.
Email: ruiwang.huang@gmail.com

Funding information
Natural Science Foundation of Guangdong Province, Grant/Award Number: 2022A1515011022; National Key Research and Development Program of China, Grant/Award Number: 2018YFC1705000; National Natural Science Foundation of China, Grant/Award Numbers: 81871338, 82171914

Abstract

Parahippocampal cortex (PHC) is a vital neural bases in spatial navigation. However, its functional role is still unclear. "Contextual hypothesis," which assumes that the PHC participates in processing the spatial association between the landmark and destination, provides a potential answer to the question. Nevertheless, the hypothesis was previously tested using the picture categorization task, which is indirectly related to spatial navigation. By now, study is still needed for testing the hypothesis with a navigation-related paradigm. In the current study, we tested the hypothesis by an fMRI experiment in which participants performed a distance estimation task in a virtual environment under three different conditions: landmark free (LF), stable landmark (SL), and ambiguous landmark (AL). By analyzing the behavioral data, we found that the presence of an SL improved the participants' performance in distance estimation. Comparing the brain activity in SL-versus-LF contrast as well as AL-versus-LF contrast, we found that the PHC was activated by the SL rather than by AL when encoding the distance. This indicates that the PHC is elicited by strongly associated context and encodes the landmark reference for distance perception. Furthermore, accessing the representational similarity with the activity of the PHC across conditions, we observed a high similarity within the same condition but low similarity between conditions. This result indicated that the PHC sustains the contextual information for discriminating between scenes. Our findings provided insights into the neural correlates of the landmark information processing from the perspective of contextual hypothesis.

KEYWORDS
contextual hypothesis, distance estimation, fMRI, landmark processing, parahippocampal cortex

1 | INTRODUCTION

Landmarks are objects in the environment that have a consistent relationship with specific locations (Epstein et al., 2017). In a spatial navigation, the landmarks are crucial for efficient wayfinding (Fischer et al., 2020) which requires a variety of spatial skills to work together (Wolbers & Hegarty, 2010). Distance estimation, one of the basic spatial skills for the successful wayfinding (Persichetti & Dilks, 2016), is believed to be benefited with the present of the landmarks (X. Chen et al., 2017; X. Chen et al., 2019). Studying the neural correlates of

the landmark-based distance estimation is profound to deepen our understanding to the human spatial navigation.

The parahippocampal cortex (PHC) is an important area for using the landmarks. In human studies, the PHC was generally delineated as the posterior section of the parahippocampal gyrus (Baumann & Mattingley, 2021). A neural recording study in epilepsy patients showed that the cells in the PHC had a high firing rate when the subjects were viewing a landmark (Arnold & Johnston, 2003). Studies also showed that the PHC was activated by salience objects from the surrounding (Janzen & van Turennout, 2004; Ramanoel et al., 2020) and was involved in reorientation using the landmark (Sutton et al., 2012). Our previous meta-analysis, which encompassed 19 fMRI experiments, showed that the PHC is involved in the navigational task using the landmark-based strategy (Qiu et al., 2019). Although the activation of the PHC was observed in landmark-based navigation, it is still unclear about the specific functions of the PHC in processing the landmark information.

The "contextual hypothesis," which proposed by Aminoff et al. (2013), may be suitable to explain the role of the PHC for landmark information processing. The hypothesis indicates that the "landmark" should be considered within the context, which is defined by the association between the object and destination (Chan et al., 2014). For example, a library could be only defined as a landmark when our destination is located in the university campus rather than outside the campus. According to the hypothesis, the PHC's involvement in contextual process is mainly manifested in two aspects: (i) The PHC activity is elicited in strong associated context than the weak one (Baumann & Mattingley, 2016). For example, the landmark would elicit the stronger PHC activity than nonlandmark object. (ii) The PHC is involved in defining the important objects for navigation scene understanding or landmark identification (Epstein & Vass, 2014). For example, Marchette et al. (2015) found that the multi-voxel pattern in the PHC decodes the familiar landmark from different views. The difference between information extraction and scene understanding is that the latter only points out the landmark in the environment (Dilks et al., 2021), while the former uses the reference of the landmarks for navigation (Aguirre et al., 1996). However, barely evidence about the contextual hypothesis is based on the spatial navigation task. Thus, an empirical study is required to test the hypothesis from the spatial navigation aspect.

In this study, we conducted an fMRI task called "Pick Up Sam" to test the contextual hypothesis based on its two aspects. Participants were requested to recall the distance after a short period of encoding under three conditions: landmark free (LF), stable landmark (SL), and ambiguous landmark (AL). The AL is an object that has the same appearance with the landmark in SL condition, but its location is inconstant during the navigation. Through introducing the AL condition and using the LF condition as the baseline, we can make an inference of the PHC's involvement between strong and weak object-scene association by comparing the PHC activity of the SL-versus-LF and AL-versus-LF contrasts. For testing scene understanding, we assessed the representational similarity of the three conditions in the PHC to see if its activity pattern could differentiate the conditions.

2 | MATERIALS AND METHODS

2.1 | Participants

Thirty-one right-handed healthy adult students and postgraduates (twenty females, mean age = 20.6 years) were recruited for the present study. The participants' eyesight was normal or corrected to normal. The study was approved by the Institutional Research Ethics Committee of South China Normal University (SCNU). The participants signed consent forms before the study.

2.2 | Materials

We developed an experimental task "Pick Up Sam" as the distance-estimation paradigm for measuring the distance perception of participants with or without a landmark (Bigel & Ellard, 2000). We referred to the paradigms used in previous studies (Baumann et al., 2010; Chen et al., 2020) to ensure that our task could measure the landmark-based distance estimation. In the experiment scenario, the participants drove a car to pick up a friend named Sam. In each trial, the location of Sam was randomly assigned, and the participants were required to remember and estimate the straight-line distance from a constant start position to the location.

The task was presented in a 3D virtual environment (VE) which was built with Unity 3D (version 2017, https://unity.com/). The VE sceneries are built on a meadow of 200 m × 100 m (in unity meters) with a 200 m long road running through it vertically. A car, a church, a character, and a house were the 3D objects in the VE (Figure 1a). The testing distance (TD) was defined as the length of the route from the position of the car to that of the character down the road (Figure 1a). The church served as the visual landmark. The house placed behind the character served to emphasize the character's position.

2.3 | Procedure

First, the participants were trained outside of the scanner to familiarize themselves with the task requirements. They went through a full run of the "Pick Up Sam." The participants were sent to the MRI scanner after they confirmed they understood the task verbally. In the scanner, the participants needed to complete three runs of the experimental task.

"Pick Up Sam" contains three conditions: LF, SL, and AL. Throughout these conditions, the character was kept on the right side of the road. The landmark (the church) was supplied to the participants on the left side of the road in both SL and AL, but it was not given to the participants in LF. In SL, the landmark was set 80 m away from the starting point to make sure that it could be seen constantly. In AL, the landmark was initialized in 80 m from the car, but its location changed as the car hurtled away. In the fMRI scanner, each run contained a total number of 30 trials, including 10 trials for each condition.

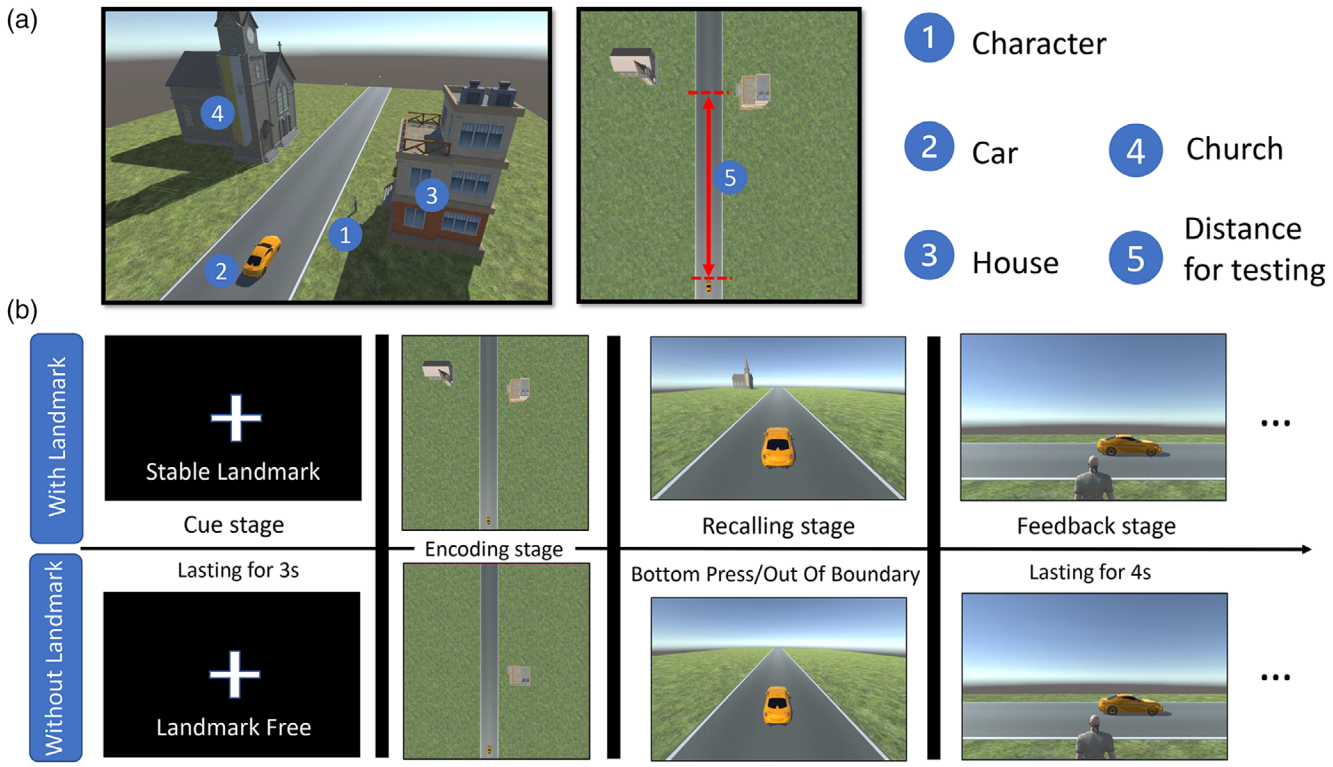

FIGURE 1 Task flow of "Pick Up Sam." The picture depicts the construction of the scene and the task flow of a single trial. (a) 3D objects used in a virtual environment. Sam and his house appeared on the right side of the road, while the church was on the left side. The red double-sided arrow shows the testing distance that the participants needed to remember. (b) The task flow is presented in two folds, with landmark (stable landmark and ambiguous landmark condition) or without landmark (landmark-free condition).

Figure 1b shows the task flow of an example trial. Each trial began with a cue stage, which was a black screen with a white cross in the middle of the screen and a texture to signify the condition ("LF," "SL," or "AL") for a duration of 3 s. This was followed by an encoding stage in which the participants witnessed the entire scene from a bird's-eye view for a duration of 5 s. Afterward, it was a recalling stage, in which the participants' vision was altered to a third-person view back from the car, and the car began autonomously driving forward down the road. Meanwhile, the character and the house vanished. The participants pressed a button to bring the car to a halt on where they felt the character was and the screen would appear to a scene for the feedback stage. In the feedback stage, the participants' perspective switched to the character's third-person perspective. In this way, the participants could check if they had stopped the car at the proper spot from this vantage point. The feedback stage lasted 5 s before moving on to the next trial.

The data were recorded in each trial, including the identification of the present condition, the length of TD, and the inaccuracy of the estimated distance. The inaccuracy was measured by the absolute value of the TD subtracting the estimated distance. To obtain a high power in the effect detection, we binarized the TD into "shortTD" and "longTD" when we programmed the task. The "shortTD" refers to $30 \leq TD < 50$ virtual meters, and the "longTD" to $50 \leq TD \leq 80$ virtual meters. In the analysis, this binary TD was used to examine the effect on the behavioral and fMRI data.

2.4 | MRI data acquisition

All imaging data were collected on a 3 T Siemens Prisma^{fit} scanner with a 64-channel phased-array head/neck receiver coil. The fMRI data were obtained using a single-shot simultaneous multi-slice or multiband gradient-echo EPI sequence with the following parameters: repetition time (TR) = 1500 ms, echo time (TE) = 31.0 ms, flip angle = 70°, slice acceleration factor = 3, field of view (FOV) = 211 mm × 211 mm, data matrix = 88 × 88, slice thickness = 2.4 mm without inter-slice gap, voxel size = (2.4 mm)^3, anterior-to-posterior phase encoding direction (A> > P), and 60 interleaved slices covering the whole brain. The functional images were acquired while the participants were performing the task. To correct for susceptibility-induced geometric distortions and signal loss in the acquired functional images, we also acquired the field map of the whole brain by using a double-echo FLASH sequence with the following parameters: TR = 620 ms, TE1/TE2 = 4.92 ms/7.38 ms, flip angle = 60°, FOV = 211 mm × 211 mm, voxel size = (2.4 mm)^3, and 60 axial slices. In addition, high-resolution brain structural images were acquired using a T1-weighted 3D MP-RAGE sequence with the following parameters: TR = 1800 ms, TE = 2.07 ms, flip angle = 9°, slice thickness = 0.8 mm, FOV = 256 mm × 256 mm, data matrix = 320 × 320, voxel size = (0.8 mm)^3, and 208 sagittal slices covering the whole brain.

2.5 | Functional data preprocessing

The data sets from two participants were discarded due to their head motion during scanning (mean FD > 0.2 mm and max FD > 5 mm). Thus, a total of 29 participants' data were used in the following statistics. Functional images were preprocessed using fMRIPrep (ver 20.1.1) (Esteban et al., 2019). The steps included: (1) signal distortion correction with fieldmap, (2) slice-time correction, (3) head-motion correction by six parameters, (4) resample into a $(2\ mm)^3$ standard MNI space, (5) spatial smoothing with an isotropic, Gaussian kernel of 6 mm full-width half-maximum, and (6) motion artifacts removal using ICA-AROMA. The images without spatial smoothing and ICA-AROMA were also obtained for performing representational similarity analysis (RSA). Afterward, a high band pass-filter of 1/100 Hz and denoising the confounds from the preprocessed fMRI images were conducted using an open-source python script (https://github.com/arielletambini/denoiser). The confounds included the signals of brain white matter and cerebrospinal fluid.

2.6 | Behavioral analysis

The inaccuracy of distance estimation was initially log-transformed to shape its distribution to a normal distribution. The influence of task conditions (three levels: SL, AL, LF) and TD (two levels: shortTD and longTD) on the inaccuracy was estimated using a linear mixed-effect model (LMM). The task conditions, TD and their interaction were introduced as the fixed effect in the LMM, and the random interception of each participant was introduced as the random effect in the LMM. The key feature of the landmark-based distance estimation is about using the external ref provided by the landmark (X. Chen et al., 2019). Thus, the participants' estimation to the distance was expected to be more precise with the present of a landmark relative to the LF condition. The LMM parameters were estimated using the *lmeTest* package (Kuznetsova et al., 2017) in R language.

2.7 | Univariate statistical analysis for the fMRI data

We examined the PHC activity in different contexts using general linear model (GLM) with parametric modulations. The encoding stage reflects the encoding of the distance with or without a landmark, and the recalling stage represents the maintaining of the information, as the working memory. Therefore, we modeled the brain activity in encoding (GLM1) and recalling stage (GLM2), respectively. We focus on the effect of the landmark, so the LF condition was chosen as the baseline.

For GLM1, the first-level analysis included 10 regressors: r1–r3 were the main effect of each condition in the encoding stage; r4–r6 were the modulatory effect of the TD length in each condition in the encoding stage; r7–r10 were the main effect of the recalling stage, cue stage, feedback stage, and ending stage. The modulation effects, r4–r6, modeled the changes in brain activity with TD length and directly reflected the encoding of the distance information.

For GLM2, the first-level analysis was built similarly to GLM1, except for the switch from the encoding stage to the recalling stage. In particular, the 10 regressors were as follows: (r1–r3) were the main effects of three conditions in recalling stage; (r4–r6) were the modulatory effects of TD length in the corresponding condition in recalling stage; and the encoding, cue, feedback, and ending stages were (r7–r10). We used the modulatory of TD to model the maintaining of the distance information.

The "short TD" was labeled as 1, and the "long TD" as 2 for modeling the brain activity increased with the distance length. All modulatory regressors were set to orthogonalize to their constant regressor manually. For instance, the modulation effect in the LF condition was orthogonalized to the main effect of the LF condition.

In the group-level analysis, we assessed the SL-versus-LF contrast (SL > LF) with respect to the modulation effects. As a control, we also estimated the AL-versus-LF contrast (AL > LF) to see if the PHC would be activated by a nonlandmark object. The group-level analyses for the GLM1 and GLM2 were conducted under the same pipeline, which was as follows: The estimations of the brain activation from the first-level analysis were assembled and a paired *t* test was conducted to determine the significant brain activity throughout the whole brain. The statistical threshold was set at the voxel-level $p < .001$ (uncorrected for multiple comparisons) with a cluster size ≥20 voxels.

Our consideration for comparing the modulatory effects rather than the main effects were twofold: First, the behavioral analysis estimated impact of the interaction between the task condition and TD to the participants' judgment. Thus, using the modulatory effects in the GLMs allowed us to optimize the comparability between the behavioral and brain activity results. Second, the SL/AL condition has a landmark, but the LF condition does not. Thus, the effect may interference by the visual effect if comparing the main effect directly.

To obtain more power for detecting the PHC activity, we also conducted a small volume FWE correction for the group-level inference in the bilateral PHC masks. The PHC masks were defined based on the Human Brainnetome Atlas (Fan et al., 2016), including the left PHC (120 voxels, MNI: −19, −12, −30) and right PHC (179 voxels, MNI: 19, −10, −30).

In addition to the voxel-wise approach, we also performed an ROI-based analysis to directly compare the activity in the PHC across different conditions by using a repeated measures ANOVA. To begin, the left and right PHC masks were defined according to the Human Brainnetome Atlas (Fan et al., 2016), and the beta-value estimated by the first-level GLMs was transformed into a *z*-value by Fisher's *z*-transformation. Then, to obtain the PHC activity, we extracted the *z*-values of the modulation effect and averaged it within the PHC masks. Finally, the repeated measures ANOVA was performed to assess the differences in the PHC activations across the conditions. The pair-wise difference was assessed using a paired *t* test corrected by the Holm method (Holm, 1979). The ROI-based analysis was conducted separately for each ROI (left and right PHC) and GLM (GLM1 and GLM2).

The first- and group-level GLM analysis were performed using FSL/Feat software (https://fsl.fmrib.ox.ac.uk/fsl/fslwiki/FEAT). The repeated measures ANOVA and pairwise comparison were conducted by R package ggstatsplot (Patil, 2018).

2.8 | Representational similarity analysis

To test whether the PHC contributed to scene understanding, we performed an ROI-based RSA. The PHC needed to meet two criteria to be determined whether it "knows" the scene: (1) It would have to be sensitive to the identification of the scene. And (2) it would be able to identify whether an object is navigationally relevant. Thus, we designed the hypothetical scene-specificity representational dissimilarity matrices (sRDM, Figure 2 left panel) to characterize the similarity pattern according to the scene understanding. sRDM had high similarity when representing the same condition and low similarity when representing different conditions.

To determine the specificity of the PHC in scene understanding, we introduced two additional RDMs that were unrelated to scene understanding. (i) a visual-specificity RDM (vRDM, Figure 2 middle panel) to describe visual processing: We assumed that the vRDM would have a high similarity between SL and AL because they had an identical object (the church) in the scene and (ii) the task-specificity RDM (tRDM, Figure 2 right panel) to describe the contexts of the task demand. We assumed that the tRDM had a high similarity between the LF and AL conditions because they had an identical task demand ("distance estimation without landmarks").

To obtain the neural activity in different conditions using RSA, we reran the first level of the GLM1 with unsmoothed fMRI data. We used the GLM1 instead of the GLM2 because the landmark identification occurs at the beginning of the navigation (R. A. Epstein & Vass, 2014). The main effects of each condition, instead of the modulation effects, were used as the inputs the activity pattern for RSA because the distance length was not necessary for the landmark recognition.

The first-level analysis of the ROI-based RSA was performed as follows: First, the beta value for each voxel within the ROI was extracted for each condition across three runs, resulting in a neural activity matrix of nine rows and N_{voxel} columns. Then, we calculated the pairwise Pearson's correlation between each row of the neural activity matrix to obtain a 9 × 9 representational similarity matrix (RSM). The correlations in the RSM were transferred into the correlation distance ($1 - r$) as a measure of the neural RDM, and the representational similarity between the neural RDM and each theoretical RDM was estimated by the Pearson's correlation. In the group-level analysis, a nonparametric permutation test was performed on the first-level representational similarities to determine whether the representational similarity was significantly greater than 0 (5000 permutations). Then, the p values from the permutation test were corrected by the Bonferroni multiple comparisons correction (six comparisons: three RDMs × two ROIs).

A whole-brain searchlight was also performed to explore the similarity pattern by a data-driven method. The searchlight was conducted with a 4 mm radius sphere within the brain grey matter, which was defined by FSL's standard mask, and separated by each RDM to obtain the whole-brain RSA maps. Then, the RSA maps were transformed by Fisher's z value and smoothed by a 4 mm full-width half-maximum kernel. Afterward, the RSA maps were assembled for group inference using one-sample permutation test and FWE correction for multiple comparison correction. The RSA estimation software was provided by the R-package rMVPA (Buchsbaum, 2019).

3 | RESULTS

3.1 | Behavioral results

The median of the participants' recalling distance was 47.42 m, and the median of inaccuracy was 2.57 m (Figure S1b,c). LMM analysis found the interaction effect of the task condition and TD had a significant influence on the inaccuracy of estimation (Table S1). Specifically, for the LF and AL conditions, the inaccuracy of estimation in the long TD was significantly higher than that in the short TD (LF: $t_{2760} = 7.46$, $p_{Bonferroni} < .001$; AL: $t_{2758} = 6.07$, $p_{Bonferroni} < .001$, Figure 3). Meanwhile, the inaccuracy of estimation in the SL condition was significantly lower than that in the LF and AL conditions for long TD (SL > LF: $t_{2759} = -7.09$, $p_{Bonferroni} < .001$; SL > AL: $t_{2758} = -6.32$, $p_{Bonferroni} < .001$, Figure 3).

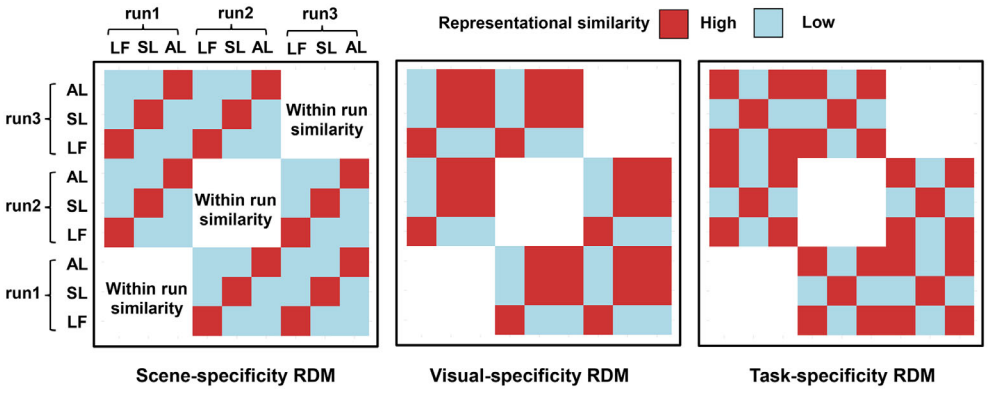

FIGURE 2 Illustration of predefined representational dissimilarity matrices (RDMs). These RDMs were used to detect the pattern similarity in the representational similarity analysis (RSA). The blanks in each matrix stand for the within-run similarity which were omitted in the RSA because we focused on the between-run similarity.

3.2 | Brain areas related to distance encoding

Figure 4a shows the brain clusters with significant activity for the SL-versus-LF contrast in the encoding stage. Two clusters were observed in the anterior and posterior left PHC (anterior: cluster size = 55 voxels, peak *z*-value = 4.24; posterior: cluster size = 31 voxels, peak *z*-value = 3.98). We also obtained two widespread clusters centering in the left lingual gyrus (cluster size = 1569 voxels, peak *z*-value = 5.63) and right occipital lobe (cluster size = 1490 voxels, peak *z*-value = 6.12) which showed a stronger response in the encoding than in the recalling stage. Using a small volume correction with the bilateral PHC masks, we identified two clusters located in the anterior and posterior left PHC (anterior: cluster size = 21 voxels, peak *z*-value = 4.22; posterior: cluster size = 7 voxels, peak *z*-value = 3.67).

For the AL-versus-LF contrast, we identified a cluster with significant activity in the right lingual gyrus (cluster size = 26 voxels, peak *z*-value = 3.79) in the encoding stage. No significant clusters were observed for the bilateral PHC masks after small volume correction.

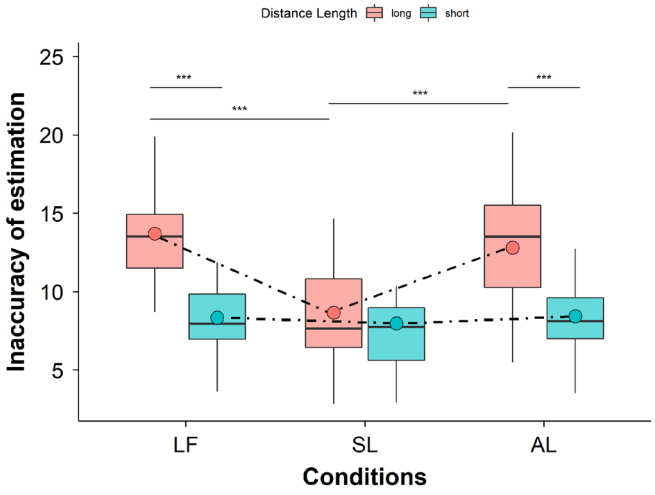

FIGURE 3 Inaccuracy of estimation in different conditions with different lengths. The inaccuracy of estimation is grouped by the task condition (landmark free [LF], stable landmark [SL], and ambiguous landmark [AL], the x axis) and distance length (short and long). The outsize dots represent the mean value of inaccuracy of estimation in its group. The vertical line through the box shows the range of the inaccuracy, and the horizontal line in the box represents the median of the data. The border of the box shows the interquartile range of the data which the upper border stands for the 75th percentile and the lower border for 25th percentile. The statistical significance of the difference between groups is marked above the dots. "***," *p* value < .001 after Bonferroni correction

3.3 | Brain areas related to information maintaining

Figure 4b shows the clusters with significant activity for the SL-versus-LF contrast in the recalling stage. We did not observe significant activity in the PHC but found three clusters with significant activity in the left hippocampus (cluster size = 29, peak *z*-value = 4.24), right middle frontal cortex (cluster size = 392, peak *z*-value = 4.93), and right cingulate gyrus (cluster size = 85, peak *z*-value = 4.11). We also observed responses of the bilateral retrosplenial cortex in a vast cluster (cluster size = 3465, peak *z*-value = 5.61).

For the AL-versus-LF contrast, we found a cluster with significant activity in the left middle temporal gyrus in the same stage (cluster size = 110 voxels, peak *z*-value = 3.93). No significant cluster was identified after small volume correction.

3.4 | PHC activation across conditions

The average activity in the left PHC was significantly different across conditions in the encoding stage ($F = 5.42$, $p < .01$, $\eta^2 = 0.16$, 95% CI = [0.02, 0.33]), and a pair-wise comparison showed higher activation in the SL condition than in the LF and AL conditions (Figure 5b).

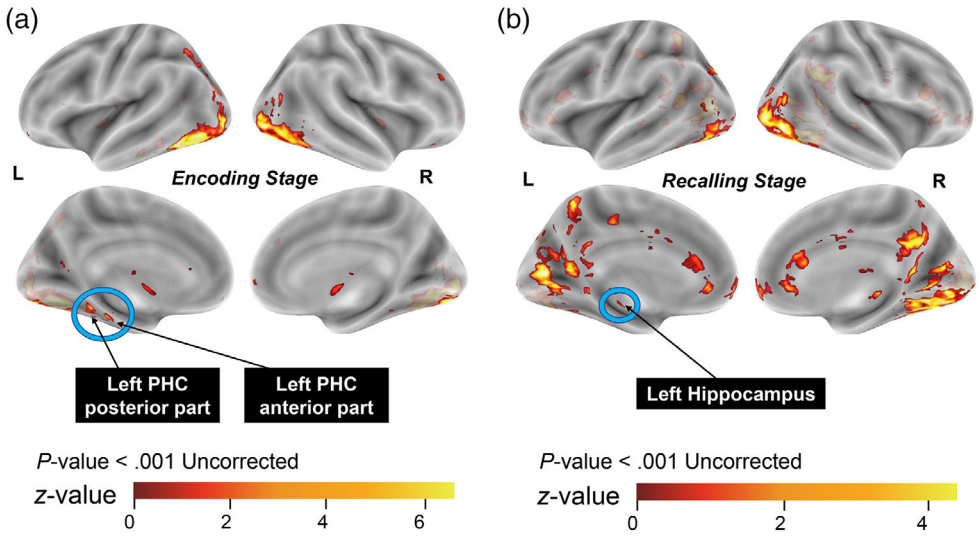

FIGURE 4 Significant areas obtained from the stable landmark (SL)-versus-landmark-free (LF) contrast based on general linear models (GLMs). The brain areas with significant activation with respect to the modulation effect of testing distance in the SL > LF contrast are indicated by blue circles. (a) Significant activations in the distance encoding stage and (b) the recalling stage. The color bar indicates the z-values for the voxels.

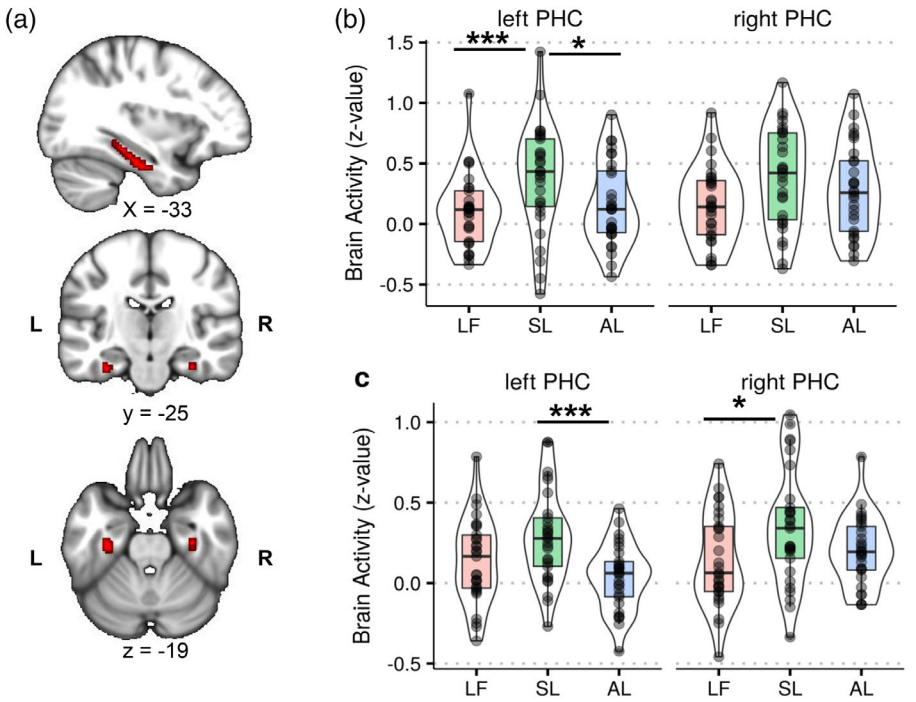

FIGURE 5 Activation of the bilateral parahippocampal cortex (PHC) between three different conditions. (a) The bilateral PHC masks. They were determined using the Human Brainnetome Atlas (Fan et al., 2016). (b) The differences in activity of the PHC for the encoding stage across all of the participants, and (c) same to (b) but for the recalling stage. "*," $p < .05$ and "***," $p < .001$ after Holm correction. AL, ambiguous landmark condition; LF, landmark-free condition; SL, stable landmark condition

No significant difference was observed in the right PHC across conditions.

We detected that the PHC activation differed significantly across conditions in the recalling stage, for either the left side ($F = 8.28$, $p < .01$, $\eta^2 = 0.23$, 95% CI = [0.05, 0.40]) or the right side ($F = 3.93$, $p = .02$, $\eta^2 = 0.12$, 95% CI = [0.00, 0.28]). The left PHC's activation in the SL condition was higher than that in the AL condition. Also, the right PHC's activation was higher in the SL condition than in the LF condition (Figure 5c).

3.5 | Similarity patterns between neural response and theoretical RDMs

For the ROI-based RSA, Figure 6a shows that the sRDM significantly accounted for the pattern similarity in the left PHC (similarity = 0.01, 95% CI = [0.008, 0.015], $p_{Bonferroni} = .018$, Cohen's $d = 0.6$) but not for the vRDM (similarity = 0.03, 95% CI = [0.013, 0.043], $p_{Bonferroni} = .366$, Cohen's $d = 0.36$) or tRDM (similarity = −0.01, 95% CI = [−0.025, −0.003], $p_{Bonferroni} = 1$, Cohen's $d = -0.24$). The activity pattern in the right PHC did not show significant similarity with any of the RDMs.

The whole-brain searching again showed the pattern similarity in the left PHC could be accounted by the sRDM rather than the other two RDMs (Figure 6b). We found that the sRDM also explained the neural pattern in parietal cortex, fusiform gyrus, and occipital cortex. The pattern in the occipital cortex was explained by the vRDM. No cluster was detected with the tRDM. The detailed information for significant clusters in the whole-brain searching RSA is listed in Tables S3 and S4 (Supplementary Materials).

4 | DISCUSSION

The current study tested the contextual hypothesis for the PHC's involvement in using the landmark-based strategy with a novel distance estimation task named "Pick Up Sam." The participants completed a series of distance estimations under three conditions: LF, SL, and AL conditions. We found that the inaccuracy of estimation was lower in the SL condition compared with the other two conditions when the participants recalled a relatively long distance. The fMRI data showed the PHC was activated by the SL condition when encoding the distance, but not by a the AL condition. Further, the representation of the task conditions was encoded differently in the PHC.

4.1 | The landmark improves the distance estimation

The behavioral analysis showed that the presence of an stable land will increase the accuracy in the distance estimation (Figure 3), indicating that the participants indeed used the landmark to assist their distance estimation. This result is consistent with that of previous studies (Ekstrom et al., 2018; Gramann et al., 2017; Janzen & Jansen, 2010; Kapaj et al., 2021). Specifically, the landmark seems to suppress the accumulating path integration errors which refers the declined accuracy in distance estimation and orientation over the long distance (Heinze et al., 2018).

Indeed, we found that the suppression of the accumulating error by the landmark was more obvious over a relatively long TD (>50 m, Figure 4) than a relatively short distance (≦50 m in our task). The interaction of distance and condition may suggest the reference of a

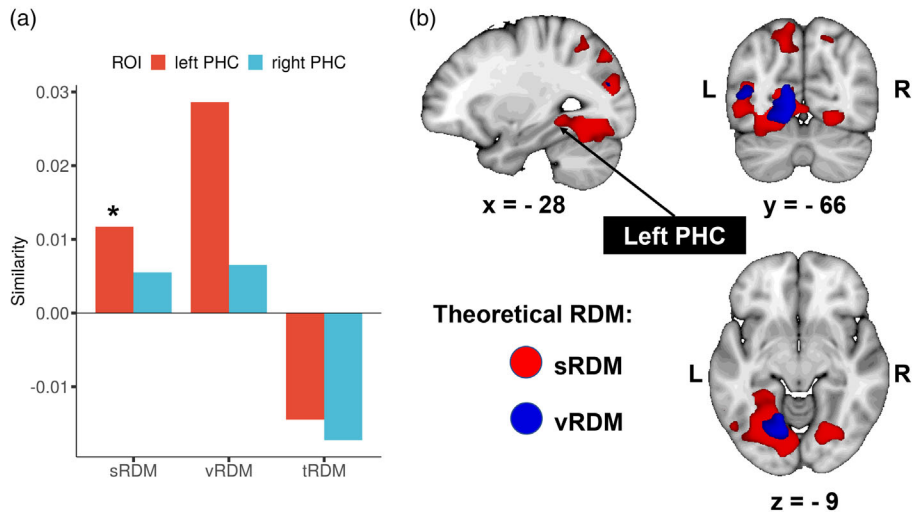

FIGURE 6 Pattern similarity in the ROI-based and searchlight representational similarity analysis (RSA) analyses. (a) The ROI-based RSA result in the parahippocampal cortex (PHC). The y axis shows the pattern similarity (Pearson's correlation) between the neural activity within the PHC's ROI and three theoretical representational dissimilarity matrices (RDMs). The x axis shows the identifications of the theoretical RDMs. "*," $p < .05$ after Bonferroni correction. (b) The significant clusters obtained from the whole-brain searchlight RSA ($p < .05$ with the FWE correction). Clusters in different colors indicate the results corresponding to specific RDM. "sRDM" stands for the scene-specificity RDM, "vRDM" for visual-specificity RDM, and "tRDM" for task-specificity RDM

landmark would drop to the baseline (LF condition) when the destination is too far away from the landmark. Studies also showed that the spatial reference provide by a landmark is available where the target is located nearby (Manley et al., 2021), and the landmark-goal integration would breakdown when the distance between them is too large (Jetzschke et al., 2017).

4.2 | PHC activity and the landmark-based strategy

We observed an increased activity of the left PHC in SL-versus-LF contrast but did not find the identical effect in AL-versus-LF contrast in the distance encoding phase (Figure 4a). This result is in line with the contextual hypothesis which suggests that the strong context rather than the weak context would elicit the activity of the PHC (Aminoff et al.. 2013). In "Pick Up Sam," the spatial association between the SL and destination is stronger than that between AL and destination. The PHC activation in landmark context may reflect its involvement in encoding landmark reference for navigation, which is consistent with the previous study showing that the PHC encoded the target position with landmarks (Sommer et al., 2005; Wegman et al., 2014).

In the recalling stage, we found significant activity difference in the PHC for the SL-versus-LF contrast from the ROI-based GLM analysis (Figure 5c) but not from the voxel-wise GLM analysis (Figure 4b). This discrepancy may be resulted from the different detection sensitivity or statistical power between the two approaches. Thus, we are unable to conclude that the PHC involves in maintaining information.

4.3 | PHC's involvement in scene understanding

The RSA revealed that the representation of task conditions was encoded differently in the PHC (Figure 6). Ruling out the possibilities about visual processing (vRDM) and task processing (tRDM), the RSA results revealed that the PHC represents the contextual information about the current scene which suggests the PHC could identify the landmark from the surroundings. This finding is consistent with the previous studies showing that the PHC participates in identifying layout-defining scene features (Mullally & Maguire, 2011), and encoding navigationally relevant objects (Janzen & van Turennout, 2004).

It is worth to note that the whole-brain searching revealed that the scene-categorization effect was detected in the posterior PHC, which refers to the parahippocampal place area (PPA) in a prior study (Epstein & Kanwisher, 1998). Studies showed that the PPA was a critical area to scene-categorization (Julian et al., 2017; Troiani et al., 2014). However, we did not localize the PPA in the current study. Therefore, we must be careful in interpreting the RSA result in the function of the PHC instead of the PPA.

Combining the results from the GLMs and RSA, our findings supported the contextual hypothesis, which proposes the PHC participates in identifying the landmark-scene association and binding their information in as a context while the hippocampus maintains the landmark-destination association in working memory to guide the navigation. Furthermore, we found the anterior part of the PHC dominated the information extraction (Figure 4a) while its posterior part participated in scene understanding (Figure 6b), which may suggest functional segregation along the anterior–posterior or axis, as the previous studies (Aminoff et al., 2007; Baumann & Mattingley, 2021).

4.4 | Extra PHC contributions to the landmark information processing

The PHC activity obtained from GLM and RSA provides the evidence to test the contextual hypothesis. We observed significant activity in other regions beyond the PHC from the GLMs and RSA, such as the hippocampus, medial prefrontal cortex (mPFC), lateral occipital cortex (LOC), and the lingual and fusiform gyrus, in the landmark-based distance estimation.

The hippocampus and mPFC all showed increased activity for the SL-versus-LF contrast throughout the recall stage (Figure 4b). The hippocampus is considered as the center for processing of spatial working memory (Baddeley et al., 2011), and the mPFC was found in recalling the target location (Patai & Spiers, 2021). These regions were found to compose a network in response to the proximity of the goal (Viard et al., 2011). Previous studies showed that their connectivity supported the memory retrieval in navigation (Liu et al., 2018; Zielinski et al., 2020). Therefore, the activation in the hippocampus and mPFC may reflect the higher memory load in the landmark condition, which the participants needed to keep the information from both the landmark and goal.

From GLM1 and GLM2 analyses, we found significant activity in the LOC in response to the SL-versus-LF contrast (Figure 4b,c), which is a major area for visual object processing (Nagy et al., 2012). When we performed an ROI-based GLM analysis in the occipital place area (OPA), which is a scene-selective region in the LOC, we detected no significant difference in activation in the OPA between different conditions in the encoding stage (Figure S2 in the Supplementary Materials). This discrepancy may reflect the functional specificity of the PHC in the landmark-based distance estimation. However, the contextual hypothesis assumes that the LOC may couple with the PHC to form a network for processing the context (Aminoff et al., 2013), and study revealed that the PHC had widespread connections with the occipital areas (Baldassano et al., 2013; Baldassano, Esteva, Li & Beck, 2016). Therefore, we infer that the LOC and the PHC may work together to accomplish the landmark information processing in the distance estimation, which could be tested with a connectivity method in future study.

The lingual and fusiform gyrus had significantly activation from both GLMs (Figure 4) and RSA (Figure 6b). Previous studies suggested that the increased activity in these regions may be related to paying attention to a landmark (Janzen & Jansen, 2010; Janzen & Weststeijn, 2007). Also, the lingual and fusiform gyrus were found to be involved in the size perception for 3D objects (Weidner et al., 2014). In "Pick Up Sam," the optic flow is the only internal cue that the participants could use for the distance estimation. Thus, we infer that these regions may be recruited by the demands of visual information processing.

4.5 | Distance estimation-related brain activity

The distance estimation may involve some other regions which were detected using GLM2 (the recalling stage). We found that the activity of the LOC and retrosplenial cortex (RSC) in the recalling stage (Figure 4b), which suggests these regions were recruited by the distance estimation. Previous study showed that the LOC participates in selecting the objects that are salient to a goal (Dilks et al., 2013). Persichetti and Dilks (2016) found that the LOC and RSC are sensitive to the egocentric distance. In the recalling stage, the participant was viewing the scene from a third-person perspective back from the car, which could be seen as an egocentric reference. A previous study found that the RSC was activated in the translation transformation of viewpoint, making the information available from the various perspective (Lambrey et al., 2012). Therefore, the RSC may be involved in transforming the distance information from the allocentric reference to the egocentric referen.

5 | LIMITATION AND CONCLUSION

The main limitation of the current study was that we only measured distance knowledge as an index of the participants' navigational performance using a distance estimation task. Distance knowledge which reflected by the accuracy in distance estimation is important for spatial navigation (Ishikawa, 2021); however, it only partially reflects navigational ability. To get a full picture of landmark-based navigation, future studies would benefit from utilizing broader measurements of navigational performance, such as direction sense, reorientation, or the wayfinding process.

The lateralization of the brain areas in spatial navigation was observed in our study. The effects in the left PHC were identified in either the univariable analysis, or the RSA, while no effect was detected in the right PHC. The lateralization is often seen in spatial navigation (Epstein et al., 2017; Iglói et al., 2010). In our previous meta-analysis, we found the existence of lateralization among 47 fMRI studies in spatial navigation (Li et al., 2021). However, to discuss the lateralization is out of the scope of the current study, and we hope a future study could dig into this topic.

In conclusion, we studied the role of the PHC in landmark information processing based on the contextual hypothesis with a navigation-relevant task named "Pick Up Sam." The presence of the landmark enhanced the participants' performance in distance judgment. The PHC was activated by the landmark, not the nonlandmark object when encoding the distance. However, we did not identify the activity of the PHC in information maintaining. When assessing the multi-voxel pattern similarity, we found the neural activity pattern in the PHC identified the task conditions, suggesting that the PHC could clarify the very scene of the experiment and recognize the landmark in the environment. Our study provided evidence for supporting the contextual hypothesis in explaining the PHC's involvement in the landmark-based distance estimation.

ACKNOWLEDGMENTS

The work was supported by funding from the Natural Science Foundation of Guangdong Province (2022A1515011022), National Natural Science Foundation of China (Grant numbers: 82171914 and 81871338), the National Key Research and Development Program of

China (2018YFC1705000). The authors thank Professor Bradley Buchsbaum for providing the RSA software. The authors appreciate Rhoda E. Perozzi and Edmund F. Perozzi, PhDs, for editing the manuscript.

CONFLICT OF INTEREST

The authors declare no competing conflict of interests.

DATA AVAILABILITY STATEMENT

All codes used in the present study are available on Gitee repository (https://gitee.com/qunjunliang/pick-up-same-analysis-scripts). The data that support the findings of this study are available from the corresponding author upon reasonable request.

ORCID

Qunjun Liang https://orcid.org/0000-0002-7610-9649
Ruiwang Huang https://orcid.org/0000-0002-5126-516X

REFERENCES

Aguirre, G. K., Detre, J. A., Alsop, D. C., & D'Esposito, M. (1996). The parahippocampus subserves topographical learning in man. *Cerebral Cortex*, *6*(6), 823–829. https://doi.org/10.1093/cercor/6.6.823

Aminoff, E., Gronau, N., & Bar, M. (2007). The parahippocampal cortex mediates spatial and nonspatial associations. *Cerebral Cortex*, *17*(7), 1493–1503. https://doi.org/10.1093/cercor/bhl078

Aminoff, E. M., Kveraga, K., & Bar, M. (2013). The role of the parahippocampal cortex in cognition. *Trends in Cognitive Sciences*, *17*(8), 379–390. https://doi.org/10.1016/j.tics.2013.06.009

Arnold, D. H., & Johnston, A. (2003). Motion-induced spatial conflict. *Nature*, *425*(6954), 181–184. https://doi.org/10.1038/nature01955

Baddeley, A., Jarrold, C., & Vargha-Khadem, F. (2011). Working memory and the hippocampus. *Journal of Cognitive Neuroscience*, *23*(12), 3855–3861. https://doi.org/10.1162/jocn_a_00066

Baldassano, C., Beck, D. M., & Li, F.-F. (2013). Differential connectivity within the parahippocampal place area. *NeuroImage*, *75*, 228–237. https://doi.org/10.1016/j.neuroimage.2013.02.073

Baldassano, C., Esteva, A., Li, F.-F., & Beck, D. M. (2016). Two distinct scene-processing networks connecting vision and memory. *eNeuro*, *3*(5), ENEURO.0178–ENEU16.2016. https://doi.org/10.1523/eneuro.0178-16.2016

Baumann, O., Chan, E., & Mattingley, J. B. (2010). Dissociable neural circuits for encoding and retrieval of object locations during active navigation in humans. *NeuroImage*, *49*(3), 2816–2825. https://doi.org/10.1016/j.neuroimage.2009.10.021

Baumann, O., & Mattingley, J. B. (2016). Functional organization of the parahippocampal cortex: Dissociable roles for context representations and the perception of visual scenes. *The Journal of Neuroscience*, *36*(8), 2536–2542. https://doi.org/10.1523/JNEUROSCI.3368-15.2016

Baumann, O., & Mattingley, J. B. (2021). Extrahippocampal contributions to spatial navigation in humans: A review of the neuroimaging evidence. *Hippocampus*, *31*(7), 640–657. https://doi.org/10.1002/hipo.23313

Bigel, M. G., & Ellard, C. G. (2000). The contribution of nonvisual information to simple place navigation and distance estimation: An examination of path integration. *Canadian Journal of Experimental Psychology*, *54*(3), 172–185. https://doi.org/10.1037/h0087339

Buchsbaum, B. (2019). rMVPA: Multivoxel pattern analysis in R (version R package version 0.1.2). Retrieved from https://github.com/bbuchsbaum/rMVPA

Chan, E., Baumann, O., Bellgrove, M. A., & Mattingley, J. B. (2014). Negative emotional experiences during navigation enhance parahippocampal activity during recall of place information. *Journal of Cognitive Neuroscience*, *26*(1), 154–164. https://doi.org/10.1162/jocn_a_00468

Chen, P. A., Jolly, E., Cheong, J. H., & Chang, L. J. (2020). Intersubject representational similarity analysis reveals individual variations in affective experience when watching erotic movies. *NeuroImage*, *216*, 116851. https://doi.org/10.1016/j.neuroimage.2020.116851

Chen, X., McNamara, T. P., Kelly, J. W., & Wolbers, T. (2017). Cue combination in human spatial navigation. *Cognitive Psychology*, *95*, 105–144. https://doi.org/10.1016/j.cogpsych.2017.04.003

Chen, X., Vieweg, P., & Wolbers, T. (2019). Computing distance information from landmarks and self-motion cues—Differential contributions of anterior-lateral vs. posterior-medial entorhinal cortex in humans. *NeuroImage*, *202*, 116074. https://doi.org/10.1016/j.neuroimage.2019.116074

Dilks, D. D., Julian, J. B., Paunov, A. M., & Kanwisher, N. (2013). The occipital place area is causally and selectively involved in scene perception. *The Journal of Neuroscience*, *33*(4), 1331–1336. https://doi.org/10.1523/JNEUROSCI.4081-12.2013

Dilks, D. D., Kamps, F. S., & Persichetti, A. S. (2021). Three cortical scene systems and their development. *Trends in Cognitive Sciences*, *26*, 117–127. https://doi.org/10.1016/j.tics.2021.11.002

Ekstrom, A. D., Spiers, H. J., Bohbot, V. D., & Rosenbaum, R. S. (2018). *Human spatial navigation*. Princeton University Press.

Epstein, R., & Kanwisher, N. (1998). A cortical representation of the local visual environment. *Nature*, *392*(6676), 598–601. https://doi.org/10.1038/33402

Epstein, R. A., Patai, E. Z., Julian, J. B., & Spiers, H. J. (2017). The cognitive map in humans: Spatial navigation and beyond. *Nature Neuroscience*, *20*(11), 1504–1513. https://doi.org/10.1038/nn.4656

Epstein, R. A., & Vass, L. K. (2014). Neural systems for landmark-based wayfinding in humans. *Philosophical Transactions of the Royal Society of London. Series B, Biological Sciences*, *369*(1635), 20120533. https://doi.org/10.1098/rstb.2012.0533

Esteban, O., Markiewicz, C. J., Blair, R. W., Moodie, C. A., Isik, A. I., Erramuzpe, A., Kent, J. D., Goncalves, M., DuPre, E., Snyder, M., Oya, H., Ghosh, S. S., Wright, J., Durnez, J., Poldrack, R. A., & Gorgolewski, K. J. (2019). fMRIPrep: A robust preprocessing pipeline for functional MRI. *Nature Methods*, *16*(1), 111–116. https://doi.org/10.1038/s41592-018-0235-4

Fan, L., Li, H., Zhuo, J., Zhang, Y., Wang, J., Chen, L., Yang, Z., Chu, C., Xie, S., Laird, A. R., Fox, P. T., Eickhoff, S. B., Yu, C., & Jiang, T. (2016). The human brainnetome atlas: A new brain atlas based on connectional architecture. *Cereb Cortex*, *26*(8), 3508–3526. https://doi.org/10.1093/cercor/bhw157

Fischer, L. F., Mojica Soto-Albors, R., Buck, F., & Harnett, M. T. (2020). Representation of visual landmarks in retrosplenial cortex. *eLife*, *9*, e51458. https://doi.org/10.7554/eLife.51458

Gramann, K., Hoepner, P., & Karrer-Gauss, K. (2017). Modified navigation instructions for spatial navigation assistance systems lead to incidental spatial learning. *Frontiers in Psychology*, *8*, 193. https://doi.org/10.3389/fpsyg.2017.00193

Heinze, S., Narendra, A., & Cheung, A. (2018). Principles of insect path integration. *Current Biology*, *28*(17), R1043–R1058. https://doi.org/10.1016/j.cub.2018.04.058

Holm, S. (1979). A simple sequentially rejective multiple test procedure. *Scandinavian Journal of Statistics*, *6*, 65–70.

Iglói, K., Doeller, C. F., Berthoz, A., Rondi-Reig, L., & Burgess, N. (2010). Lateralized human hippocampal activity predicts navigation based on sequence or place memory. *Proceedings of the National Academy of Sciences of the United States of America*, *107*(32), 14466–14471. https://doi.org/10.1073/pnas.1004243107

Ishikawa, T. (2021). Spatial thinking, cognitive mapping, and spatial awareness. *Cognitive Processing*, *22*(1), 89–96. https://doi.org/10.1007/s10339-021-01046-1

Janzen, G., & Jansen, C. (2010). A neural wayfinding mechanism adjusts for ambiguous landmark information. *NeuroImage*, *52*(1), 364–370. https://doi.org/10.1016/j.neuroimage.2010.03.083

Janzen, G., & van Turennout, M. (2004). Selective neural representation of objects relevant for navigation. *Nature Neuroscience*, *7*(6), 673–677. https://doi.org/10.1038/nn1257

Janzen, G., & Weststeijn, C. G. (2007). Neural representation of object location and route direction: An event-related fMRI study. *Brain Research*, *1165*, 116–125. https://doi.org/10.1016/j.brainres.2007.05.074

Jetzschke, S., Ernst, M. O., Froehlich, J., & Boeddeker, N. (2017). Finding home: Landmark ambiguity in human navigation. *Frontiers in Behavioral Neuroscience*, *11*, 132. https://doi.org/10.3389/fnbeh.2017.00132

Julian, J. B., Ryan, J., & Epstein, R. A. (2017). Coding of object size and object category in human visual cortex. *Cerebral Cortex*, *27*(6), 3095–3109. https://doi.org/10.1093/cercor/bhw150

Kapaj, A., Lanini-Maggi, S., & Fabrikant, S. I. (2021). *The influence of landmark visualization style on expert wayfinders' visual attention during a real-world navigation task*. UC Santa Barbara: Center for Spatial Studies. https://doi.org/10.25436/E2NP44

Kuznetsova, A., Brockhoff, P. B., & Christensen, R. H. B. (2017). lmerTest package: Tests in linear mixed effects models. *Journal of Statistical Software*, *82*(13), 1–26. https://doi.org/10.18637/jss.v082.i13

Lambrey, S., Doeller, C., Berthoz, A., & Burgess, N. (2012). Imagining being somewhere else: neural basis of changing perspective in space. *Cereb Cortex*, *22*(1), 166–174. https://doi.org/10.1093/cercor/bhr101

Li, J., Zhang, R., Liu, S., Liang, Q., Zheng, S., He, X., & Huang, R. (2021). Human spatial navigation: Neural representations of spatial scales and reference frames obtained from an ALE meta-analysis. *NeuroImage*, *238*, 118264. https://doi.org/10.1016/j.neuroimage.2021.118264

Liu, T., Bai, W., Xia, M., & Tian, X. (2018). Directional hippocampal-prefrontal interactions during working memory. *Behavioural Brain Research*, *338*, 1–8. https://doi.org/10.1016/j.bbr.2017.10.003

Manley, E., Filomena, G., & Mavros, P. (2021). A spatial model of cognitive distance in cities. *International Journal of Geographical Information Science*, *1-23*, 2316–2338. https://doi.org/10.1080/13658816.2021.1887488

Marchette, S. A., Vass, L. K., Ryan, J., & Epstein, R. A. (2015). Outside looking in: Landmark generalization in the human navigational system. *The Journal of Neuroscience*, *35*(44), 14896–14908. https://doi.org/10.1523/JNEUROSCI.2270-15.2015

Mullally, S. L., & Maguire, E. A. (2011). A new role for the parahippocampal cortex in representing space. *The Journal of Neuroscience*, *31*(20), 7441–7449. https://doi.org/10.1523/jneurosci.0267-11.2011

Nagy, K., Greenlee, M. W., & Kovacs, G. (2012). The lateral occipital cortex in the face perception network: An effective connectivity study. *Frontiers in Psychology*, *3*, 141. https://doi.org/10.3389/fpsyg.2012.00141

Patai, E. Z., & Spiers, H. J. (2021). The versatile Wayfinder: Prefrontal contributions to spatial navigation. *Trends in Cognitive Sciences*, *25*, 520–533. https://doi.org/10.1016/j.tics.2021.02.010

Patil, I. (2018). "ggstatsplot": 'ggplot2' based plots with statistical details. CRAN. https://doi.org/10.5281/zenodo.2074621

Persichetti, A. S., & Dilks, D. D. (2016). Perceived egocentric distance sensitivity and invariance across scene-selective cortex. *Cortex*, *77*, 155–163. https://doi.org/10.1016/j.cortex.2016.02.006

Qiu, Y., Wu, Y., Liu, R., Wang, J., Huang, H., & Huang, R. (2019). Representation of human spatial navigation responding to input spatial information and output navigational strategies: An ALE meta-analysis. *Neuroscience and Biobehavioral Reviews*, *103*, 60–72. https://doi.org/10.1016/j.neubiorev.2019.06.012

Ramanoel, S., Durteste, M., Becu, M., Habas, C., & Arleo, A. (2020). Differential brain activity in regions linked to visuospatial processing during landmark-based navigation in young and healthy older adults. *Frontiers in Human Neuroscience*, *14*, 552111. https://doi.org/10.3389/fnhum.2020.552111

Sommer, T., Rose, M., Glascher, J., Wolbers, T., & Buchel, C. (2005). Dissociable contributions within the medial temporal lobe to encoding of object-location associations. *Learning & Memory*, *12*(3), 343–351. https://doi.org/10.1101/lm.90405

Sutton, J. E., Twyman, A. D., Joanisse, M. F., & Newcombe, N. S. (2012). Geometry three ways: An fMRI investigation of geometric information processing during reorientation. *Journal of Experimental Psychology. Learning, Memory, and Cognition*, *38*(6), 1530–1541. https://doi.org/10.1037/a0028456

Troiani, V., Stigliani, A., Smith, M. E., & Epstein, R. A. (2014). Multiple object properties drive scene-selective regions. *Cerebral Cortex*, *24*(4), 883–897. https://doi.org/10.1093/cercor/bhs364

Viard, A., Doeller, C. F., Hartley, T., Bird, C. M., & Burgess, N. (2011). Anterior hippocampus and goal-directed spatial decision making. *The Journal of Neuroscience*, *31*(12), 4613–4621. https://doi.org/10.1523/JNEUROSCI.4640-10.2011

Wegman, J., Tyborowska, A., & Janzen, G. (2014). Encoding and retrieval of landmark-related spatial cues during navigation: An fMRI study. *Hippocampus*, *24*(7), 853–868. https://doi.org/10.1002/hipo.22275

Weidner, R., Plewan, T., Chen, Q., Buchner, A., Weiss, P. H., & Fink, G. R. (2014). The moon illusion and size-distance scaling—Evidence for shared neural patterns. *Journal of Cognitive Neuroscience*, *26*(8), 1871–1882. https://doi.org/10.1162/jocn_a_00590

Wolbers, T., & Hegarty, M. (2010). What determines our navigational abilities? *Trends in Cognitive Sciences*, *14*(3), 138–146. https://doi.org/10.1016/j.tics.2010.01.001

Zielinski, M. C., Tang, W., & Jadhav, S. P. (2020). The role of replay and theta sequences in mediating hippocampal-prefrontal interactions for memory and cognition. *Hippocampus*, *30*(1), 60–72. https://doi.org/10.1002/hipo.22821

SUPPORTING INFORMATION

Additional supporting information can be found online in the Supporting Information section at the end of this article.

How to cite this article: Liang, Q., Liao, J., Li, J., Zheng, S., Jiang, X., & Huang, R. (2023). The role of the parahippocampal cortex in landmark-based distance estimation based on the contextual hypothesis. *Human Brain Mapping*, *44*(1), 131–141. https://doi.org/10.1002/hbm.26069